sciendo

M. Landowski*

Gdansk University of Technology, Faculty of Mechanical Engineering, Department of Materials Science and Welding Engineering, Narutowicza 11/12, 80-233 Gdańsk, Poland
* miclando@pg.edu.pl

INFLUENCE OF PARAMETERS OF LASER BEAM WELDING ON STRUCTURE OF 2205 DUPLEX STAINLESS STEEL

ABSTRACT

Laser welding is used in modern industry, having many advantages comparing to traditional welding technologies. Nowadays, industry sectors such as shipbuilding, automotive and aviation can't be imagined without laser processing technologies. Possibility of increase of welded joint properties, autogenous welding and high level of process automation makes the technology of laser welding perspective part of the industry. Physical multidimensional processes complexity requires a deeper understanding of the impact of laser welding parameters on the quality of welded joints for industrial implementation. The paper presents results of microstructure investigations of laser beam welded stainless steel under various welding parameters. Welded joints was achieved by Ytterbium fiber laser type without the use of the filler material. Material for test was 2205 ferritic-austenitic duplex stainless steel (DSS) plates with thickness of 8 mm in delivery condition. The objectives of this research was to investigate influence of laser welding parameters on weld geometry of butt-welded joints. Investigations of bead shape revealed correlation between laser beam focus position and weld penetration depth.

Keywords: stainless steel; duplex, microstructure; laser beam welding

INTRODUCTION

Duplex stainless steel (DSS) is a group of steels used in the chemical, marine and petrochemical industry due to its corrosion resistance comparable to austenitic steels, moderate cost and good mechanical properties [1]. DSS consist of nearly equal amounts of ferrite and austenite phase at room temperature [2]. DSS exhibits greater toughness and better weldability than ferritic stainless steel. In the last few decades ferritic-austenitic stainless steel (DSS) grades were increasingly applied in the industry to replace austenitic stainless steels. This is the result of, on the one hand, obtaining the high corrosion resistance, and on the other hand, the necessity of reducing the mass of final products while reducing the use of expensive

alloying elements like nickel. Duplex grades containing low nickel, high chromium and nitrogen content combine good corrosion resistance with a strength almost twice as high as austenitic steels at a lower price.

Many joining techniques even in extreme conditions [3,4] have been developed to perform high quality welded joints of duplex stainless steel. Laser welding combines the ability to control the shape of the weld, repeatability of the process and easy automation along with an extremely narrow heat affected zone. All these advantages cause more and more interest in using this method to join duplex stainless steels [5,6,7]. Despite the lack of laser welding recommendations for duplex stainless steels, many research teams are trying to adjust laser welding parameters for use in these applications. Fiber laser have become attractive alternatives to existing CO_2 and Nd:YAG lasers due to their higher energy efficiency and superior beam quality. The use of laser techniques is becoming more and more common. The laser beam, besides laser welding [8,9,10], is also used e.g. for laser surface melting (LSM) and alloying (LSA) [11,12]. Additionally, the laser beam is also used for hybrid methods combining the beneficial effects of laser beam welding and different arc and plasma welding processes [13]. Industrial laser welding application benefits are also lower maintenance, smaller compact design and lower cooling requirements. The inverse absorption of the laser beam in the vapour plume is proportional to the square of the laser wavelength so the absorption coefficient of fiber laser (1.07 µm) is almost 100 times less than CO_2 laser (10.6 µm) [14].

Many scientific reports describe the impact of the basic parameters of laser welding on the depth of penetration. The most frequently studied parameters are welding speed and laser beam power [15]. There are also studies on the influence of shielding gas on weld geometry [16]. Individual publications raise the subject of focusing the beam on the shape of penetration and depth of penetration [17, 18, 19, 20]. Unfortunately, the impact of this parameter has not been clearly defined. This may be due to various technical parameters of the devices. Kawahito and others in their work [21] showed that the construction of the laser head and the diameter of the supply fiber also affects the characteristic geometrical dimensions of the weld.

In the present paper, the effect of laser beam welding parameters on microstructure and weld shape was analyzed.

EXPERIMENTAL

The test material was a flat plate with thickness of 8 mm made of duplex stainless steel grade 2205 in delivery condition. A high power continuous wave Ytterbium fiber laser IPG Photonics fiber laser YLS – 6000 with a maximum power of 6 kW and a wavelength of 1070 nm was used. The joints were made at laser output power of 4 and 6 kW. The laser beam was delivered through the optical feeding fiber (transmitting fiber) of 300 µm core diameter (Figure 1).
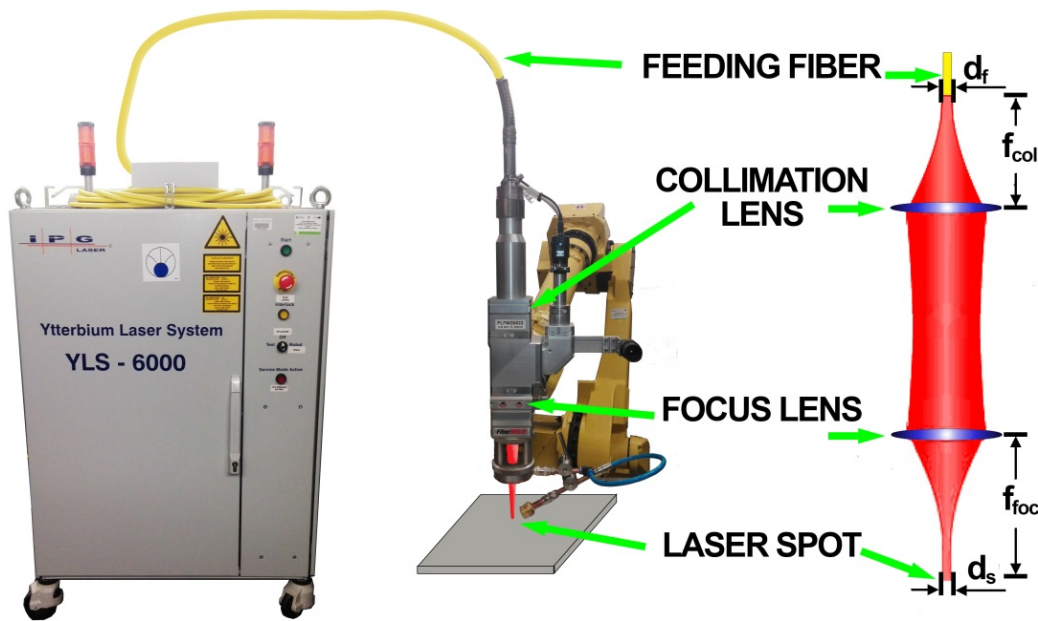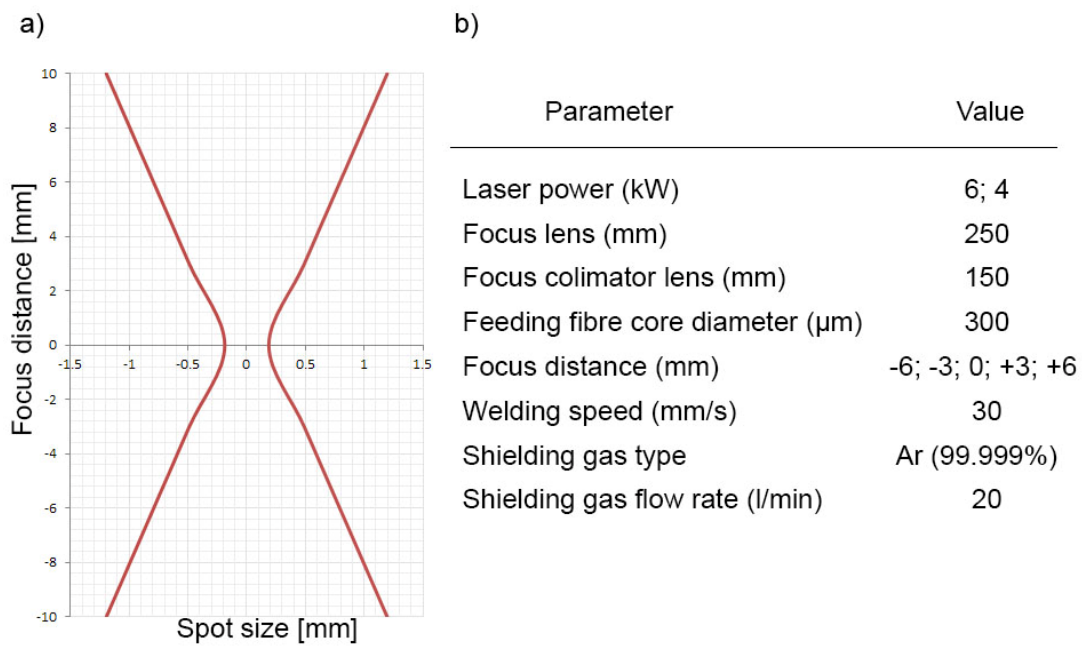
**Fig. 1.** Schematic of the experimental set-up for fiber laser welding

The focal diameter depends on the divergence angle and the beam parameter product (BPP) of the focused beam. Alternatively the optical magnification M can be used to calculate the focal spot diameter (spot size - d_s). The optical magnification depends on the design and optical properties of the collimation lens (collimation lens focus distance f_{col}) and the focus lens (focus lens focus distance f_{foc}). Focal spot diameter is given by optical magnification and feeding fiber core diameter (d_f) according to the formula (1) [22].

$$d_s = d_f * M = d_f * \frac{f_{foc}}{f_{col}} \qquad (1)$$

Welding speed was set to 30 mm/s (1.8 m/min). Welding process was carried out as autogenous - without filler metal. Argon with 99.999% purity was used as shielding gas. The flow rate was set at 20 l/min. Shielding gas was supplied by a gas nozzle mounted at laser head to avoid the oxidation of weld beads. Welding parameters used during experiment are shown in Figure 2b. The focal plane position was set -6, -3, 0, +3 and +6 mm to welded plate. Beam diameter before (+) and after (−) the focal point in the laser beam direction was diffused up to 4 times the spot diameter (Figure 2a). Fig. 3 shows how focus distance was measured - defined as the focus depth (f).

a)   b)

Parameter	Value
Laser power (kW)	6; 4
Focus lens (mm)	250
Focus colimator lens (mm)	150
Feeding fibre core diameter (µm)	300
Focus distance (mm)	-6; -3; 0; +3; +6
Welding speed (mm/s)	30
Shielding gas type	Ar (99.999%)
Shielding gas flow rate (l/min)	20

Fig. 2. Spot size in function of focus distance (a), parameter set-up for fiber laser welding (b)

f = -6 mm   f = -3 mm   f = 0 mm   f = 3 mm   f = 6 mm
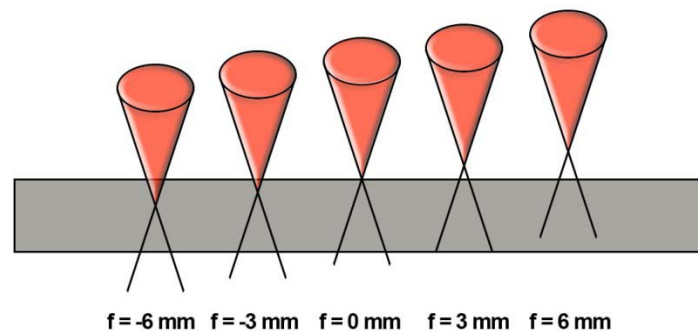
Fig. 3. Focus distance set-up for fiber laser welding

The chemical composition (Table 1) was subjected to examination using optical emission spectroscopy (PMI-MASTER-Pro by Oxford Instruments).

Table 1. *Chemical composition of 2205 (UNS S32205, EN 1.4462)*

| Chemical composition, wt.%													
C	Si	Mn	P	S	Al	B	Cr	Cu	Mo	Ni	Nb	Co	Ti
0.03	0.39	1.34	0.03	<0.003	0.0039	0.0035	22.5	0.24	3.03	5.6	0.016	0.128	<0.005

In order to prevent changes in the structure of the material under the influence of temperature during cutting, the samples for metallographic examination were cut at the cutting machine with intensive cooling. Samples were mounted in resin and ground on aqueous abrasive papers with increasing granularity from 100 to 2400 for microscopic examinations. Samples for microscopic observations were subjected to a polishing process on

a polishing cloth using an aqueous suspension of 3 µm diamonds. The metallographic samples thus prepared were subjected to etching in Beraha reagent for 30 s to reveal the microstructure of the joints in macroscopic and microscopic studies. Structural observations were carried out using light microscopy (Olympus BX51). The volume fraction of austenite in welds was measured by manual point count measurement according to ASTM E562.

RESULTS

Microscopic examination

The base material is characterized by a austenitic grains on ferrite matrix structure. Figure 4 presents the structure observed using light microscopy (LM). The gray region is the ferrite phase (δ) while the austenite phase (γ) is shown as white. As demonstrated in figure 4, continuous matrix of the δ ferrite phase surrounds the island like γ phase.
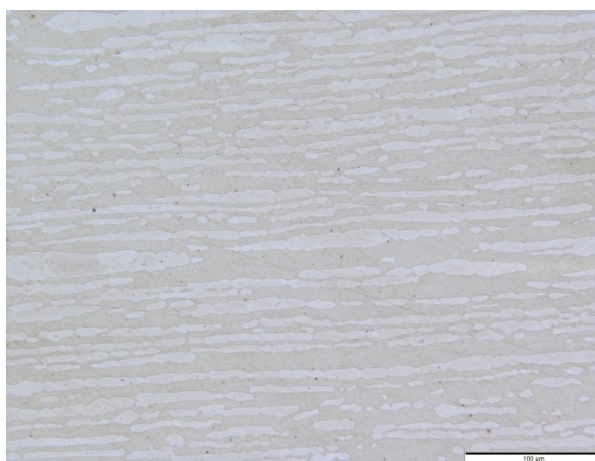
Fig. 4. Microstructure of base material. Duplex ferritic-austenitic structure. LM, mag. x200

As presented in figure 5 heat affected zone (HAZ) was barely visible. Dimensions of HAZ in laser welding is very narrow, in this case was about 10µm. Characteristic dendritic structures were observed as a result of directional crystallization caused by the direction of heat flow from liquid material of welding pool into the base material.
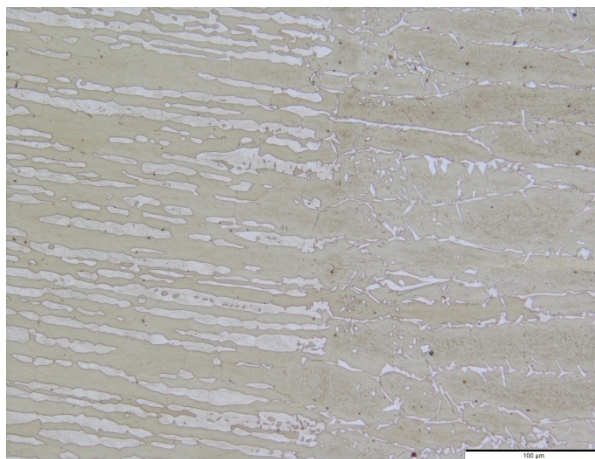
Fig. 5. Heat affected zone microstructure of laser welded joint (4 kW, f=+6 mm) mag. x200

Due to the extreme high cooling rate of the laser weld, which is the effect of heat dissipation to the base material, the structure of column crystals arranged in parallel and touching vertices in the weld axis is observed. During solidification of DSS weld metal is formed as an almost completely ferrite structure. Further during the cooling the γ phase nucleation process is initiated. As shown in figure 6 grain boundary austenite was initially formed in the interfaces between δ ferrite grains. A small amount of intragranular austenite appeared within the δ ferrite grains (Fig. 6a). The small amount of Widmanstätten austenite along the δ ferrite grain boundaries began to grow into the interior.

This can be understood by the increase of the transformation time due to increased cooling time. In this case diffusion of γ stabilizing elements such as nitrogen and nickel will be enhanced and more austenite can be transformed from δ-ferrite.
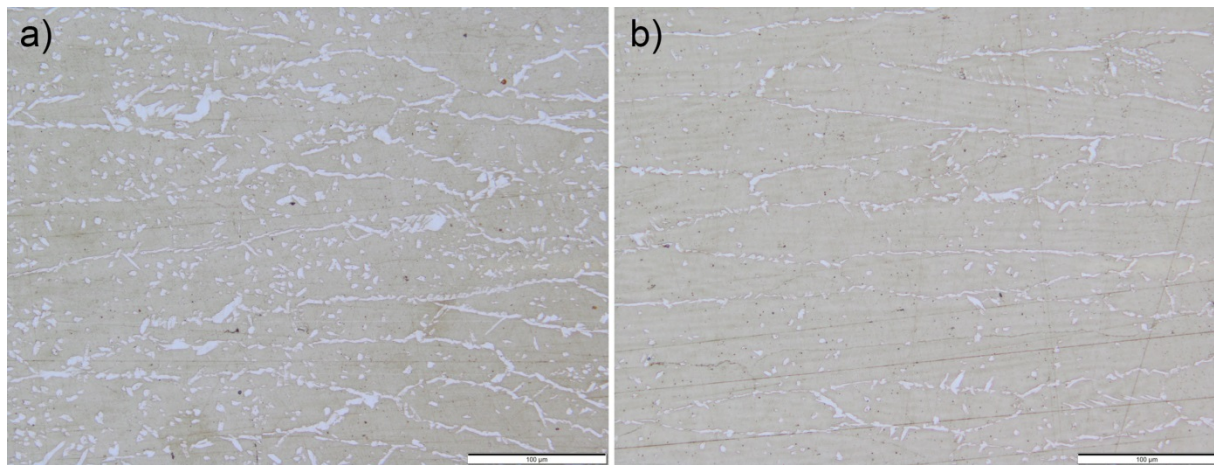
Fig. 6. Microstructure in weld zone a) 6 kW, f=-3 mm, b) 4 kW, f=-3 mm, mag. x200

The volume fraction of austenite in welds reached up to 12% measured by manual point count measurement according to ASTM E562. As presented in table 2 very high volume fraction of ferrite in weld material was obtain. This disproportion of the amount of ferrite to austenite indicates a lower corrosion resistance of the welded joint. In the case of other welding methods, a lower ferrite content was obtained for SAW 61.5%, FCAW 47%, in the case of extreme cooling rate in MMA underwater welding, 56% ferrite content was obtained.

Table 2. *Results of ferrite content measurement*

Power [kW]	Focus position				
	-6 mm	-3 mm	0 mm	+3 mm	+6 mm
4	95%	95%	90%	90%	93%
6	95%	88%	96%	96%	96%

Macroscopic examination

Figure 7a presents the macrostructure of the welded joint (laser power 6 kW, focus +6 mm) observed on the cross-section of the weld axis. The joint has a regular shape with a visible slight narrowing in the middle of the sheet thickness. Shapes of the welds are presented on figure 7b. Typical geometry of laser welded joint was observed.
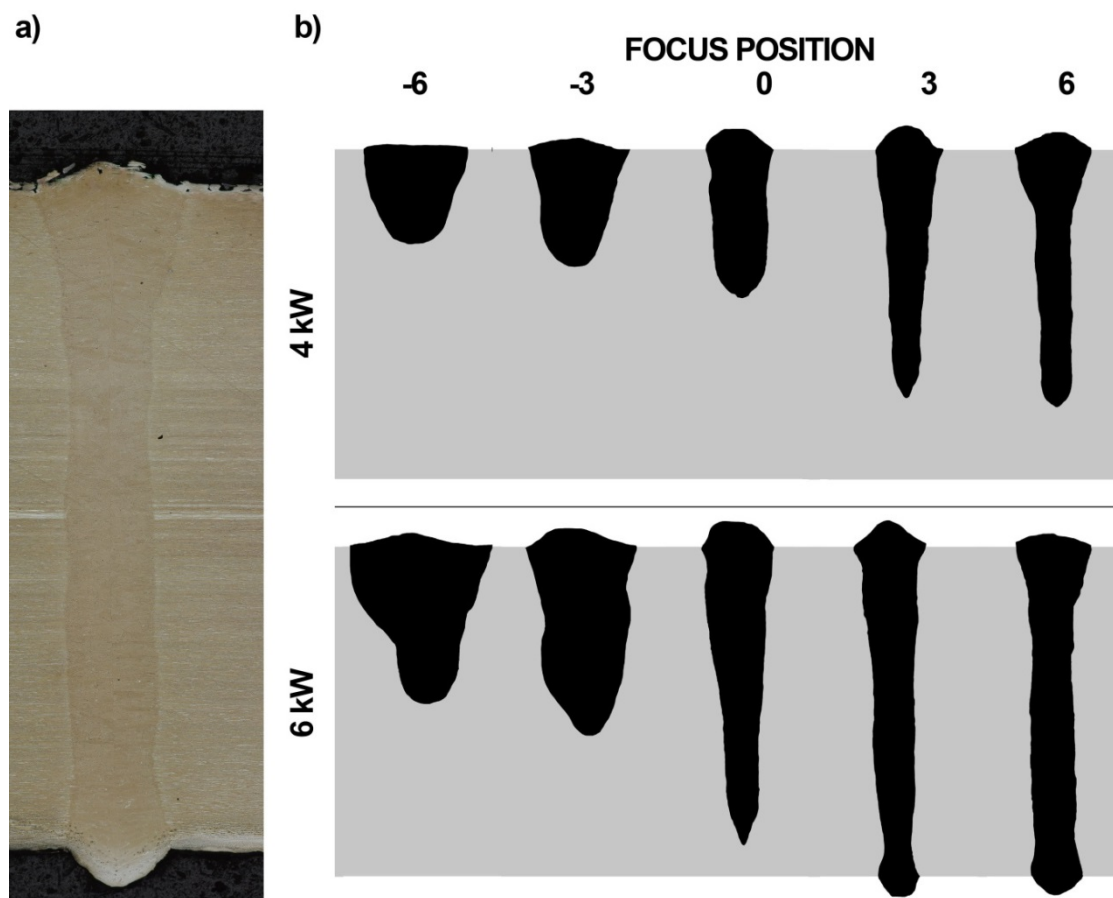
Fig. 7. Macrostructure of 2205 laser beam welded joint (a), shape of weld geometry (b)

Measurements of welds dimensions are presented in table 3. Keyhole laser welding forms a 'chalice' shaped weld bead profile. All of examined welded joints were produced without welding defects such as porosity, underfilling and humping beads. Full penetration was achieved for duplex stainless steel plate with a thickness of 8 mm at a power of 6 kW and both (3 and 6 mm) positive beam focusing positions. In the case of a positive focusing position, an increase in the depth of penetration (c) was noted. The use of a negative beam focusing position resulting in the expansion of weld bead (b) and reduce penetration depth (c). Focal position (f) change spot diameter (d_s) of laser beam which affect different heat input during welding. It can also be seen that increasing heat input by reducing the spot size (d_s) results in a reduction of the weld cross section (WA).

Statistical analyses

Module Statistica (Statsoft) was used to carry out a statistical analysis (model I – V) of data from table 3 assuming level of significance $\alpha = 0.05$. The functions describing dependent variables were determined by a simple and multidimensional regression analysis. These analyzes are commonly used to obtain mathematical models using the least squares approximation method. [23, 24]

The analysis of the statistical significance of individual tested values is presented in Figure 8 by Pareto charts. Figure 8(a–e) shows the mathematical models I, II, III, IV and V, respectively.

Table 3. Experimental conditions and results

P	f	d_S	a	b	c	d	e	WA	Schemat of laser weld geometry
kW	mm	mm	mm	mm	mm	mm	mm	mm^2	
6	-6	1.59	15.65	34.60	42.50	23.68	2.57	9.25	
6	-3	0.98	0	26.65	50.90	0	4.1	9.72	
6	0	0.38	8.11	18.18	79.84	0	5.47	8.84	
6	3	0.98	9.16	17.10	90.72	10.86	5.55	9.75	
6	6	1.59	10.25	17.90	90.40	13.04	2.78	10.14	
4	-6	1.59	16.19	26.35	26.35	7.21	0	4.81	
4	-3	0.98	0	23.28	31.71	0	2.36	5.33	
4	0	0.38	0	16.60	41.70	0	4.06	5.34	
4	3	0.98	7.82	15.52	65.67	0	6.16	6.52	
4	6	1.59	7.53	18.24	68.19	18.5	3.94	6.60	
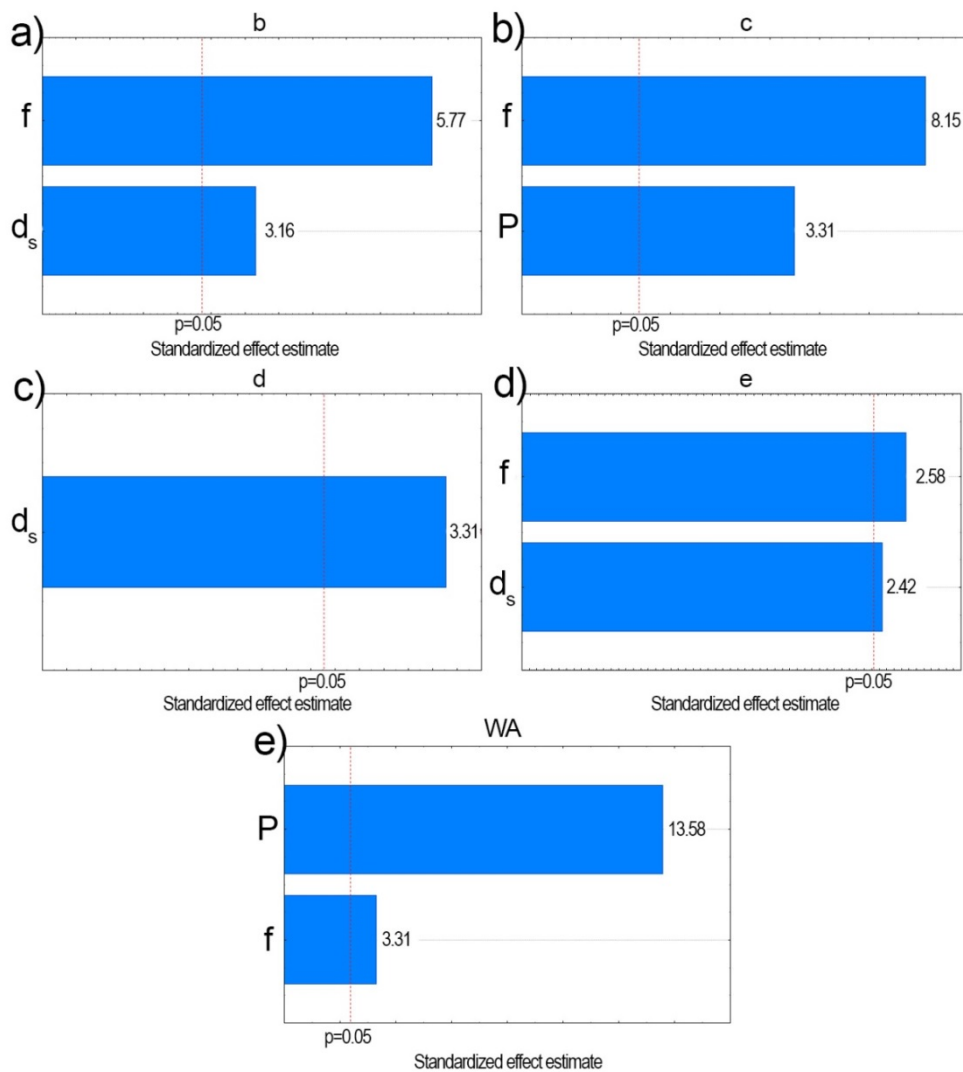
Fig. 8. Standardized Pareto charts of effects after removing of statistically insignificant values effects

The obtained mathematical models are presented in table 4. Measures of the quality of the models' match with the results of the experiment contained in table 4 show a high fit.

Table 4. *Regression equations, adequacy measures and Shapiro Wilk normality test*

Model	regression equations	R	R^2	R^2_{adj}	SW-W
Model I	$b = 15.13 - 1.12 \cdot f + 5.733 \cdot d_S$	0.93	0.86	0.82	0.97
Model II	$c = -1.57 + 12.07 \cdot P + 4.221 \cdot f$	0.97	0.93	0.91	0.87
Model III	$d = -8.19 + 14.10 \cdot d_S$	0.76	0.58	0.52	0.90
Model IV	$e = 6.181 + 0.2258 \cdot f - 2.25 \cdot d_S$	0.80	0.64	0.54	0.88
Model V	$WA = -1.92 + 1.910 \cdot P + 0.1097 \cdot f$	0.98	0.97	0.96	0.95

In addition to the substantive interpretation of the equations, the assumption of the normality of the raw residuals was assessed using the Shapiro-Wilk test [25]. Visual interpretation of test of normality is presented in Figure 9 by histograms of normality. Figure 9(a–e) shows the graphical interpretation of Shapiro-Wilk normality distribution test of mathematical models I, II, III, IV and V, respectively. All p values are greater than the significance level α, therefore these models were assumed to be correct.
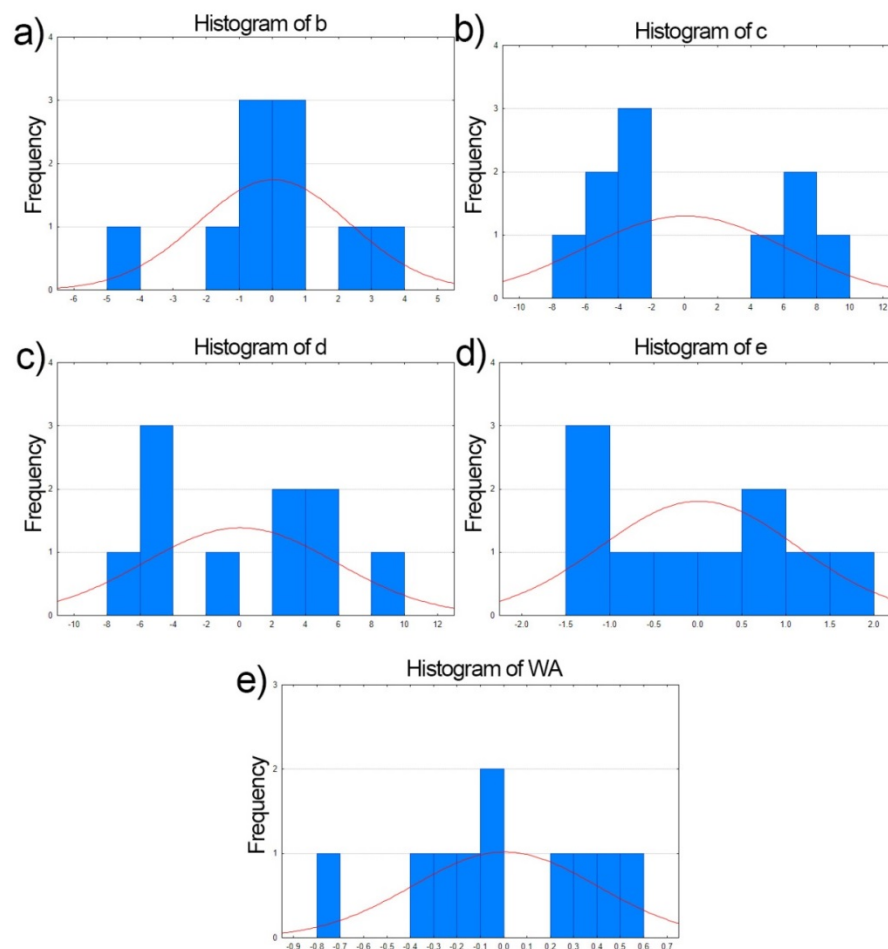
Fig. 9. Histograms of normality – Shapiro-Wilk test

CONCLUSIONS

The following conclusions were made on the basis of the conducted research:

1. The correct focusing position is one of the key parameters for shaping good quality welds. Focusing position <u>above</u> the specimen surface (+3, +6 mm) being preferable for high-power fiber laser welding of thick plates.

2. Laser welding through extremely fast heat dissipation increases the ferrite content in the welded joint, reducing the corrosion resistance of the weld.

3. Obtaining the balance ratio between ferrite and austenite is a key issue in the studies on weldability of duplex stainless steel.

4. The developed regression equations can be used to model geometries of the laser welds of thick duplex stainless steel

ACKNOWLEDGMENTS

REFERENCES

1. Zhang, Z., Jing, H., Xu, L., Han, Y., Zhao, L., & Zhou, C.: Effects of nitrogen in shielding gas on microstructure evolution and localized corrosion behavior of duplex stainless steel welding joint. Applied Surface Science 2017, 404, 110-128.

2. Varbai B., Adonyi Y., Baumer R., Pickle T., Dobránszky J., Májlinger K.: Weldability of Duplex Stainless Steels - Thermal Cycle and Nitrogen Effects. Welding Journal 2019, 98 (3), 78-87

3. Łabanowski, J., Prokop-Strzelczyńska, K., Rogalski, G., Fydrych, D.: The effect of wet underwater welding on cold cracking susceptibility of duplex stainless steel. Advances in Materials Science 2016, 16(2), 68-77.

4. Świerczyńska A, Łabanowski J, Michalska J, Fydrych D.: Corrosion behavior of hydrogen charged super duplex stainless steel welded joints. Materials and Corrosion 2017,1–9. https://doi.org/10.1002/maco.201709418

5. Qi, K., Li, R., Wang, G., Li, G., Liu, B., Wu, M.: Microstructure and Corrosion Properties of Laser-Welded SAF 2507 Super Duplex Stainless Steel Joints. Journal of Materials Engineering and Performance 2019, 28(1), 287-295.

6. Calliari, I., Gennari, C., Hurtado Delgado, E., Miranda Perez, A. F., Rodriguez Vargas, B. R.: Laser welding of plastically deformed lean duplex stainless steel. Metallurgia Italiana 2018, (1), 5-10.

7. Hu, S., Zheng, D., Zhao, G., Li, G., Tang, H.: The effect of welded joint properties on the surface characteristics of laser-welded 2205 duplex stainless steel. Advances in Mechanical Engineering 2018, 10(9), 1687814018797449.

8. Tuz, L.: Evaluation of Microstructure and Selected Mechanical Properties of Laser Beam Welded S690QL High-Strength Steel. Advances in Materials Science 2018, 18(3), 34-42.

9. Lisiecki, A.; Kurc-Lisiecka, A.: Automated Laser Welding of AISI 304 Stainless Steel by Disk Laser. Archives of Metallurgy and Materials 63 (2018), 4, 1663-1672.

10. Kurc-Lisiecka A., Lisiecki A.: Laser welding of the new grade of advanced high-strength steel Domex 960. Materiali in tehnologije / Materials and technology 51 (2017) 2, 199–204. doi:10.17222/mit.2015.158

11. Tęczar P., Majkowska-Marzec B., Bartmański M.: The influence of laser alloying of Ti13Nb13Zr on surface topography and properties. Advances in Materials Science 2019, 19(1), 44-56.

12. Janicki, D., Górka, J., Kwaśny, W., Gołombek, K., Kondracki, M., Żuk, M.: Diode laser surface alloying of armor steel with tungsten carbide. Archives of Metallurgy and Materials 2017, 62(2), 473-481.

13. Kik, T.; Górka, J.: Numerical Simulations of Laser and Hybrid S700MC T-Joint Welding. Materials 2019, 12, 516.

14. Quintino, L., Costa, A., Miranda, R., Yapp, D., Kumar, V., & Kong, C. J.: Welding with high power fiber lasers–A preliminary study. Materials & Design 2007, 28(4), 1231-1237.

15. A. Lisiecki, R. Burdzik, G. Siwiec, Ł. Konieczny, J. Warczek, P. Folęga, B. Oleksiak: Disk laser welding of car body zinc coated steel sheets. Archives of Metallurgy and Materials 2015, 60 (4), 2913–2922. DOI: 10.1515/amm-2015-0465

16. Zhang, W. W., Cong, S., Luo, S. B., Fang, J. H.: Effects of energy density and shielding medium on performance of laser beam welding (LBW) joints on SAF2205 duplex stainless steel. JOM 2018, 70(8), 1554-1559.

17. Kuryntsev, S. V., Gilmutdinov, A. K.: Welding of stainless steel using defocused laser beam. Journal of Constructional Steel Research 2015, 114, 305-313.

18. Kuryntsev S. V., Gilmutdinov A. Kh., Shiganov I. N.: Welding with a defocused laser beam, Welding International, 2017, 31:2, 151-156.

19. Metelkova J., Kinds Y., Kempen K., de Formanoir C., Witvrouw A., Van Hooreweder B.: On the influence of laser defocusing in Selective Laser Melting of 316L. Additive Manufacturing 2018, 23, 161-169.

20. Guo N., Xing X., Zhao H., Tan C., Feng J., Deng Z.: Effect of water depth on weld quality and welding process in underwater fiber laser welding. Materials & Design 2017 115, 112-120.

21. Kawahito Y., Mizutani M., Katayama S.: High quality welding of stainless steel with 10 kW high power fibre laser, Science and Technology of Welding and Joining 2009, 14:4, 288-294.

22. Abt F., Heß A., Dausinger F.: Focusing of high power single mode laser beams. ICALEO 2007, 202 (2007); doi: 10.2351/1.5061053

23. Abioye T. E., Mustar N., Zuhailawati H., Suhaina I.: Prediction of the tensile strength of aluminium alloy 5052-H32 fibre laser weldments using regression analysis. The International Journal of Advanced Manufacturing Technology 2019, 1-12.

24. dos Santos Paes L. E., Pereira M., Weingaertner W. L., Scotti A., Souza T.: Comparison of methods to correlate input parameters with depth of penetration in LASER welding. The International Journal of Advanced Manufacturing Technology 2019, 1-13.

25. Razali N. M., Wah Y. B.: Power comparisons of Shapiro-Wilk, Kolmogorov-Smirnov, Lilliefors and Anderson-Darling tests. Journal of Statistical Modeling and Analytics 2011, 2(1), 21-33.